JJBS

Volume 16, Number 2,June 2023
ISSN 1995-6673
Pages 279 – 288
https://doi.org/10.54319/jjbs/160212

Jordan Journal of Biological Sciences

Biogenic Synthesis of Chitosan/Silver Nanocomposite by *Escherichia coli* D8 (MF062579) and its Antibacterial Activity

Mohamed M. El-Zahed*, Zakaria A. M. Baka, Mohamed I. Abou-Dobara, and Ahmed K.A. El-Sayed

[1] *Department of Botany and Microbiology, Faculty of Science, Damietta University, New Damietta, Egypt.*

Received: October 18, 2022; Revised: December 12, 2022; Accepted: December 15, 2022

Abstract

Silver nanomaterials are usually applied as antimicrobial agents; however, they can cause toxic effects on human health. The current investigation was performed to study the combined effects of chitosan and silver nanoparticles (AgNPs) using the cell-free supernatant of *Escherichia coli* (MF062579). The produced chitosan/silver nanocomposite (CS/AgNC) showed good antibacterial activity and high stability. The biosynthesized CS/AgNC contained homogeneous spherical AgNPs with an average size of ~12.3 nm and a net surface charge of +30.9 ± 3.2 mV. CS/AgNC revealed a good minimum inhibitory concentration (MIC) result against Gram-negative (G-ve, *E. coli*) and Gram-positive (G+ve, *Bacillus cereus*) bacteria with inhibition ratios of 80.7% and 75.5%, respectively. Nanocomposite-treated cells displayed complete lysis of the bacterial cell, a low amount of DNA, and cell membrane and wall disruption. Glutamate dehydrogenase (GDH) and malate dehydrogenase (MDH) activities of tested bacterial strains were demonstrated using spectrophotometry and electrophoresis on a non-denaturing acrylamide gel. In CS/AgNC-treated strains, enzyme production and activity were fewer than in untreated strains. The obtained results suggested that CS/AgNC seems to be more effective against G-ve than G+ve bacteria.

***Keywords**:* silver, chitosan, nanocomposite, biosynthesis, *Escherichia coli*, antibacterial

1. Introduction

Silver (Ag) is usually applied as a disinfectant in medical equipment, antimicrobial wound dressings, food containers, and other industrial applications (Natsuki *et al*., 2015; Zhang *et al*., 2016; Kate *et al*., 2020). Continuous physical and chemical studies competed to synthesize new antimicrobial silver nanoparticles (AgNPs) as soon as nanotechnology was discovered, which proved that the properties of nanoscale materials can be very different from those at a larger scale (Bayda *et al*., 2020). However, earlier techniques were expensive, risky, challenging, and potentially harmful to both humans and the environment. Recent advances in the field of nanobiotechnology, sometimes known as "biological techniques," offer novel, simple, and quick instruments for producing AgNPs that are affordable and environmentally benign (Iravani *et al*., 2014). Microorganisms like bacteria, fungi, yeast, and algae are frequently used in biological approaches for producing AgNPs because of how easy they are to cultivate, how quickly they develop, how diverse they are, and how well they adapt to various environmental circumstances. To bio-reduce the silver ions (Ag^+) to AgNPs, one of the biological agents, bacteria, responded differently with various metal solutions (Tsekhmistrenko *et al*., 2020; Saravanan *et al*., 2021). The production of nanoparticles (NP) involves a variety of reducing biological elements, including proteins, enzymes, peptides, and pigments. Some bacteria can biosynthesize nanoparticles using either extracellular or intracellular methods with different efficiency, size, and shape. However, intracellular methods require more expensive and time-consuming extraction and additional purifying processes (Nguyen *et al*., 2022, Singh *et al*., 2020). In order to produce AgNPs and silver nanocomposites with special features, *Escherichia coli* is employed as one of the best nanofactories (El-Shanshoury *et al*., 2011, Baltazar-Encarnación *et al*., 2019, El-Zahed *et al*., 2021b). Currently, the aggregation, agglomeration, and biocompatibility of nanomaterials hinder their applications in different biomedical fields (Restrepo and Villa, 2021). The combination of AgNPs with a polymer matrix could be considered as one of the most important solutions proposed to overcome these problems (Fan *et al*., 2022).

The most prevalent and least expensive natural biopolymer, chitosan (CS), has surface functional groups that can bind with Ag^+ and other heavy metal ions. CS was used as an antibacterial agent in medicines, biosensing devices, diagnostics, etc. (Youssef & Hashim, 2020). However, a variety of parameters, including concentration, bacterial species, pH, and others, can affect the antibacterial action of CS (Menazea *et al*., 2020; Badi'ah, 2021). Combination between AgNPs and CS will enhance the composite biological, chemical, and physical qualities, including stability, catalytic activity, optical, and

* Corresponding author. e-mail: : mohamed.marzouq91@du.edu.eg.

mechanical capabilities. Chitosan/silver nanocomposite (CS/AgNC) has recently been used in antimicrobial formulations against pathogens that are harmful to people, animals, and plants (Namasivayam *et al*., 2022). CS/AgNC nanocomposite showed antibacterial activity against methicillin-resistant *Staphylococcus aureus* and found a high bactericidal impact at minimum inhibitory concentrations (MIC) of 0.25, 0.45, and 0.15 mg/mL for AgNPs, CS, and CS/AgNC solutions, respectively (Hassanen and Ragab, 2021). Additionally, Tripathi *et al*., (2014) reported using the agar diffusion method that the composite had antibacterial efficacy against *Pseudomonas aeruginosa*, *E. coli*, and *Bacillus subtilis*. The molecular analysis of CS/antibacterial AgNC's action is still very evident and is of considerable interest for both fundamental research and the creation of pharmaceutical medicines.

Thus, AgNPs were prepared using biological synthesis, integrated into the polymeric matrix of CS, and tested *in vitro* for antibacterial activity. To our knowledge, this is the first study to use glutamate dehydrogenase (GDH) and malate dehydrogenase (MDH) as models for investigating the structure-function relationships in proteins of the CS/AgNC-treated bacteria.

2. Experimental methods

2.1. The bacterial strains and culture conditions

The bacterial strains of *Bacillus cereus* ATCC 6633 and *E. coli* ATCC 25922 were obtained from the American Type Culture Collection (ATCC), USA. While the *E. coli* D8 (MF062579) strain was obtained from the Microbiology Laboratory Culture Collection (MLCC), Egypt. All bacterial strains were cultivated on tryptic soy agar (TSA, Sigma-Aldrich, USA) for 48 h at 37°C.

2.2. Synthesis of chitosan/silver nanocomposite

The biological preparation of AgNPs was carried out according to El-Dein *et al*. (2021). Briefly, 4 ml of 0.001 M $AgNO_3$ (Panreac Quimica S.L.U, Spain) and 4 ml of the cell-free supernatant of *E. coli* D8 (MF062579) were mixed, adjusted to pH 7, and submitted to the sunlight at room temperature (25°C in our case) until the appearance of a dark brown suspension showing AgNPs formation. Then, the suspension was centrifuged at 10,000 rpm twice for 10 minutes each (Eppendorf 3H24RI intelligent high-speed refrigerated centrifuge, Herexi Instrument & Equipment Company, China), and the residue was rinsed thrice with distilled H_2O to eradicate excess impurities, and then centrifuged and dried. A solution of 1% CS (w/v, MW 50–190 KDa, deacetylation degree: ≥85%, Sigma-Aldrich, USA) was prepared in 1% acetic acid (pH 8), mixed with a solution of AgNPs (596 µg/ml) in a ratio of 1:1 v/v, and then exposed it to ultrasonication for 1 hr at 25°C by using an ultrasonic bath (Delta-sonic 920 Nº484, Meaux, France, 28 kHz). A jacketed vessel containing circulated, cooled distilled water was used to maintain the temperature at 25°C (Price *et al*. 1995). After the ultrasonication time, the product was kept on a magnetic stirrer/hot plate (IKA, Germany) at 70°C with constant stirring (500 rpm) for 90 minutes. Finally, the pH of the CS/AgNC solution was adjusted to 7.5 with 0.001 M NaOH by using a pH-meter (Jenco Electronics Ltd., Micro-Computer pH Meter Model 6209), centrifuged at 10,000 rpm for 10 minutes, and then freeze-dried (Baka *et al*., 2019).

2.3. Characterization of chitosan/silver nanocomposite

The spectrum of AgNPs formation was monitored using UV-Vis spectrophotometry (Beckman DU-40). CS/AgNC were analyzed using the Malvern Zetasizer Nano-ZS90 (Malvern, UK), X-ray diffractometer (Shimadzu, Japan), and transmission electron microscopy (TEM, JEM-2100, Japan).

2.4. Silver nanoparticles release from CS/AgNC

The release of Ag^+ from CS was tested according to El-Zahed *et al*. (2021a). 50 µg/ml of AgNPs solution was prepared, added to dialysis tubes, and then submerged within 200 ml of double distilled water and incubated in a shaking incubator at 37°C/100 rpm (LSI-3016R, Daihan Lab Tech Co., Ltd., Namyangju, Kyonggi, South Korea). The released Ag^+ was evaluated using atomic absorption spectroscopy (PerkinElmer, UK) (Sotiriou *et al*., 2012).

The CS/AgNC solubility was investigated in several polar and non-polar solvents, including water, ethanol, methanol, dimethylformamide (DMF), acetone, n-butyl alcohol, toluene, and hexane (Sigma-Aldrich, USA). The Zeta average size (Zavg) and polydispersity index (PDI) were estimated using the Malvern Zetasizer.

2.5. In vitro antibacterial test using agar well diffusion method

Antibacterial experiments were conducted according to the Clinical and Laboratory Standards Institute (CLSI, Clinical and Laboratory Standards, 2007). 100 µl of each tested bacterial suspension (2.5×10^3 $CFU.ml^{-1}$); *B. cereus* ATCC 6633 and *E. coli* ATCC 25922 were added to cold melted Mueller-Hinton agar (MHA) medium (Oxoid, UK) at the time of pouring the plates in triplicate. After solidifying the agar plates, 100 µl of a unified concentration (150 µg/ml) of $AgNO_3$, CS, AgNPs, CS/AgNC and penicillin (as a positive control) was added separately into punched holes (5 mm) under aseptic conditions and incubated at 37°C for 48 hr. Then, the inhibition zones of bacterial growths were measured (mm).

2.6. Minimum inhibitory concentration

The MIC tests for treated bacteria were evaluated according to CLSI (Clinical Laboratory Standards, 2017). Different concentrations (1-30 µg/ml) of $AgNO_3$, CS, AgNPs and CS/AgNC were added into Mueller-Hinton broth (MHB) medium flasks inoculated by 2.5×10^3 $CFU.ml^{-1}$ tested bacteria and incubated at 37°C and 150 rpm for 24 hr. Untreated bacteria and penicillin were used as controls. Bacterial growth rates were measured spectrophotometrically (λ: 600 nm) against controls. The percentage growth inhibition was evaluated according to the formula: % growth inhibition = (ODc-ODt) × 100, where ODc; the optical density of broth media (negative control) and ODt is the optical density of CS/AgNC-treated bacteria.

2.7. Ultrastructural analysis of treated bacteria

The bacterial cell cultures were exposed to CS/AgNC (MIC value) for 2 hr at 37°C in MHB. Bacterial cells were washed, fixed with 2.5% glutaraldehyde and 0.1 M cacodylate buffer, pH 7, and sent to the Central Laboratory, Electron Microscope Unit, Faculty of

Agriculture, Mansoura University, Egypt, for observing and studying their ultrastructure.

2.8. Protein estimation

The bacterial protein concentration of untreated and CS/AgNC-treated strains was estimated according to Kruger (2009) method. Briefly, the bacterial strains; *B. cereus* ATCC 6633 and *E. coli* ATCC 25922 were subjected to MIC, 6 µg/ml of CS/AgNCs for 2 hr at 37°C. After that, they were harvested using a tabletop centrifuge (Centrifuge Model 800 by Xiangshui. FADA medical apparatus factory, China) for 20 minutes at 5000 rpm. The bacterial pellets were washed three times in sterile distilled water after the supernatants were discarded. The pellets were centrifuged at 10,000 rpm at 4°C after being sonicated for one minute at 750 W, 20 kHz. The supernatants were put into fresh, sterile eppendorf tubes for the upcoming assays and kept at 4°C. Additionally, untreated bacterial samples were included. The Bradford method was used to evaluate the concentration of bacterial proteins (Bradford, 1976).

2.9. Estimation of some of dehydrogenase activity

The GDH and MDH activities of the untreated and CS/AgNC-treated bacteria were assayed according to Robb *et al*. (2001) and Yoshida, (1965), respectively. Briefly, the activity of the GDH enzyme was measured spectrophotometrically by evaluation of the reduction rate of NAD^+ in a reaction mixture of 0.2 ml of NAD^+ (2 mg/ml), 0.1 ml of 1 M sodium glutamate (Oxoid, UK), 2.6 ml of 0.5 M phosphate buffer (pH 7.0) (Oxoid, UK) and 0.1 ml of bacterial enzyme solution. For the oxidation of L-malate; 2.5 ml of 0.5 M phosphate buffer (pH 7.0), 0.1 ml of 0.1 M sodium malate (Oxoid, UK), 0.1 ml of 10 mM NAD^+; 0.1 ml of enzyme solution, and water to a final volume of 3.0 ml are placed in a quartz cuvette. By measuring optical density at 340 nm, the enzymatic processes were spectrophotometrically quantified (UV-1100, Shanghai Mapada Instruments Co., Ltd., Shanghai, China). A mole of NAD^+ reduced to NADH for each unit time at 25°C was used to measure enzyme activity. The number of enzyme units per microgram of protein is how specific activity is measured.

2.10. Total Soluble protein profile by SDS-PAGE

SDS-PAGE was studied to clarify the protein profiles of untreated and CS/AgNC-treated *B. cereus* ATCC 6633 and *E. coli* ATCC 25922, according to Laemmli, (1970). Bacterial proteins were analyzed by SDS-PAGE (12% w/v polyacrylamide gel with 6% w/v stacking gel) at 150 mV in a miniprotean® 3 electrophoresis cell (BioRad, USA). Protein detection was typically done using Coomassie blue staining.

2.11. Isozymal profiles for MDH and GDH using native PAGE

Vertical PAGE was used. A 10% native polyacrylamide gel overlaid with a 6% polyacrylamide stacking gel was prepared using the electrode buffers according to Laemmli, (1970) without SDS. Electrophoresis was carried out at ≈4°C (on an ice bath) with a constant voltage of 150 mV (about 2 hr). After electrophoresis, the gels were placed directly into substrate solutions for the visualization of specific activity. For GDH, 16.9 g of sodium glutamate was added to 100 ml of 0.5 M phosphate buffer, pH 7.0. About 5 ml of substrate solution and 60 mg of NAD^+ were mixed well and completed into 100 ml by distilled water. For MDH, 1.34 g of L-malic acid was added to 4.9 ml of 2 M Na_2CO_3 and completed into 100 ml by distilled water. Then, 25 ml of phosphate buffer, 5 mL of substrate solution and 60 mg of NAD^+ were mixed well and completed to 100 ml by distilled water. Then a staining solution (30 mg of nitroblue tetrazolium (NBT) and 2 mg of phenazine methosulphate (PMS)) was added into each enzymatic reaction mixture just before incubation in the dark at 37°C until a blue color appeared (Selander *et al*., 1986). The gels were rinsed for 5 minutes in distilled water and proteins were fixed in glacial acetic acid/water (5%).

2.12. Statistical analysis

All the experiments were carried out in triplicate. Results (means ± standard deviation (SD)) were analyzed with ordinary one-way ANOVA tests (SPSS software, 18) with a statistically significant *P*-value < 0.05 (O'connor, 2000).

3. Results

3.1. Synthesis and characterization of CS/AgNC

AgNPs physical-chemical properties were characterized. AgNPs caused a surface plasmon resonance (SPR) at ≈424 nm, indicating a good dispersion of particles in the nanocolloids (Genç *et al*., 2017, Figure 1A). Size distribution by intensity and by volume determined using dynamic light scattering (DLS) (Figure 1B) and Zeta potential (Figure 1E) results confirmed the monodispersity of the produced NPs (0.316 ± 0.11 PDI) and their positive net surface charge (+21 ± 1.9 mV). While the net surface charge of CS/AgNC was increased to +30.9 ± 3.2 mV (Figure 1D). The AgNPs XRD patterns showed characteristic diffraction peaks for Ag at 2θ = 32.25°, 38.25°, 46.3°, 57.6°, and 64.55° which resemble the crystallographic planes of (110), (111), (200), (210), and (220), respectively (Figure 1C). The TEM micrograph of AgNPs showed ≈12.3 ± 2.3 nm uniform spherical particles (Figure 1F & G).

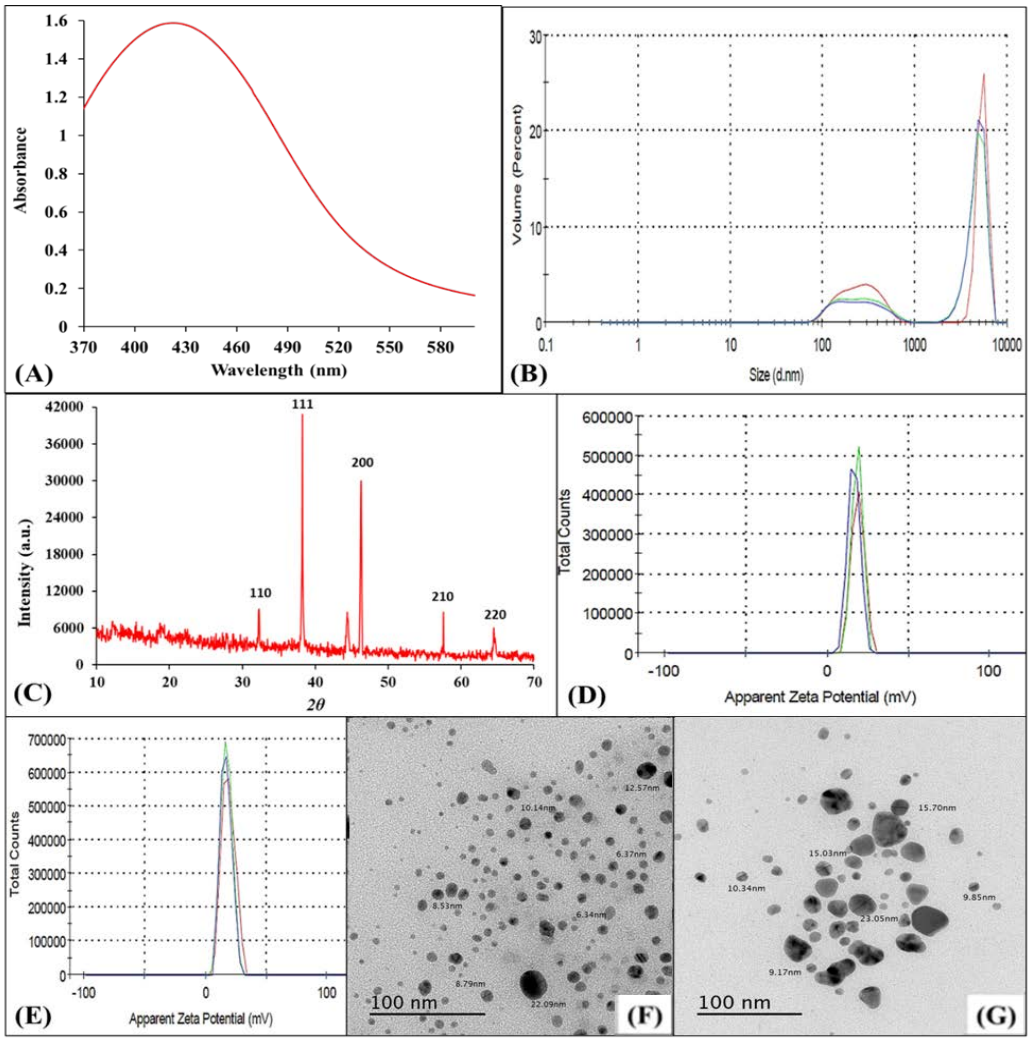

Figure 1. Chitosan/silver nanocomposite characterization. (A) UV-Vis spectrum of AgNPs. (B) Size distribution by intensity and by volume was determined using DLS measurements of AgNPs in deionized water. (C) X-ray diffraction (XRD). (D) Zeta potential of the AgNPs. (E) Zeta potential of CS/AgNC. (F) TEM micrograph of AgNPs. (G) CS/AgNC by TEM. Bars scale = 100 nm (F &G).

The presented work embedded the AgNPs into the CS, which played an important role in decreasing and delaying in silver release from the polymeric matrix (Figure 2). Zeta average size and PDI measurements for the solubility of CS/AgNC in polar and non-polar solvents confirmed that the release capacity of silver decreased in the tested non-polar solvents (Supplementary Table 1).

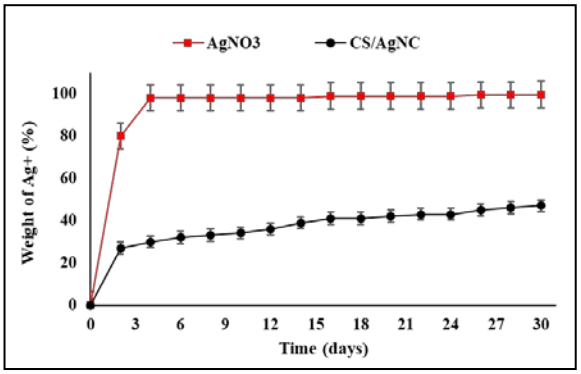

Figure 2. The release property of $AgNO_3$ and AgNPs from CS/AgNC at 37°C.

3.2. Antibacterial activity

The antibacterial activity of CS/AgNC was demonstrated and compared with the free AgNPs synthesized using the bacterial supernatant, as well as the solo polymer CS. Treatment with CS, AgNPs, and CS/AgNC inhibited the growth of all tested bacterial strains as shown in Supplementary Table 2. Results showed AgNPs and CS/AgNC had better bactericidal action against the G-ve than the G+ve bacteria.

CS/AgNC and penicillin showed the same MIC values (6 µg/ml) against *E. coli* and *B. cereus* besides complete inhibition at 25 µg/ml exhibiting a dose-dependent behavior of CS/AgNC antibacterial potential (Figure 3). The MIC value of CS/AgNC inhibited the growth of *B. cereus* by 75.5% and *E. coli* by 80.7% (Figure 4).

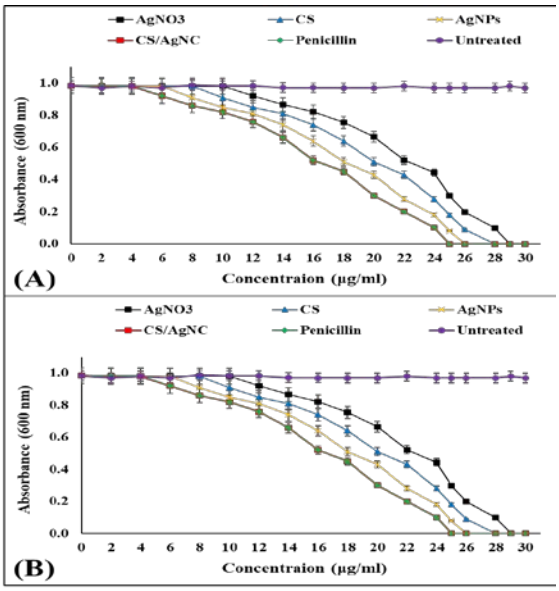

Figure 3. Effect of $AgNO_3$, CS, AgNPs, CS/AgNC and penicillin against the broth cultures of *B. cereus*; (A) and *E. coli*; (B).

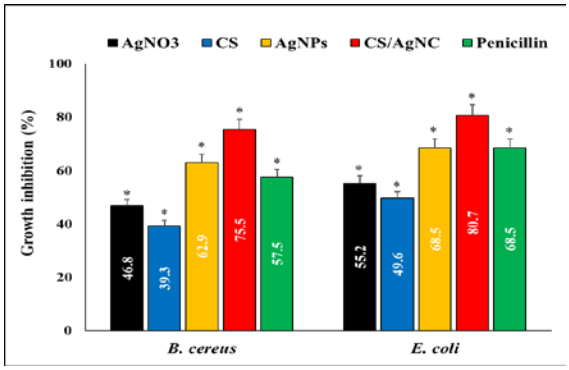

Figure 4. Growth inhibition percentage of $AgNO_3$, CS, AgNPs, CS/AgNC and penicillin against *B. cereus* and *E. coli* strains (Highly significant = * $P < 0.05$, n = 3). Ultrastructural changes in treated bacteria

3.3. Ultrastructural changes in treated bacteria

Morphological characteristics of the ultrastructure of *B. cereus* cells in MHB changed in response to their treatment with CS/AgNC (Figure 5). Native cells were identical rods with integral cell walls (Figure 5A). The CS/AgNC-treated cells showed damaged and crinkled cell walls, as well as a separation between them and the plasma membrane was observed (Figure 5B & C).

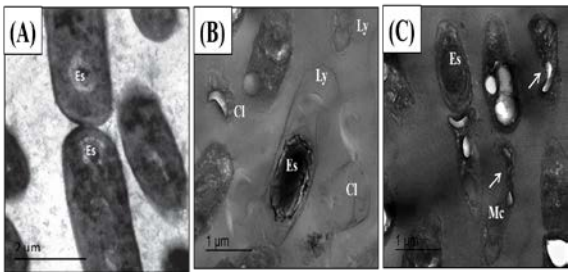

Figure 5. TEM micrograph of the bactericidal effect of CS/AgNCs on the ultrastructure of *B. cereus*. (A) A negative control (without CS/AgNCs). (B & C) A treated sample (at 6 µg/ml), there are irregular-shaped rods (arrows) with lysed cell walls (Ly), malformed cells (Mc), and complete cell lysis (Cl). Note the endospore formation (Es).

Figure 6 shows the negative effects of CS/AgNC on the ultrastructure of *E. coli*. Untreated cells appeared as uniformly dense rods. In contrast, the CS/AgNC-treated cells displayed damaged cells with irregular shapes in addition to an obvious rupture between their cell membrane and cell wall (Figure 6B).

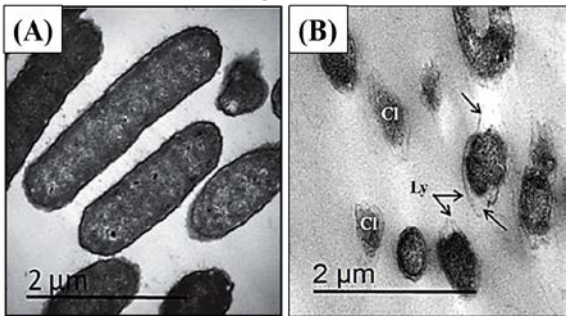

Figure 6. TEM micrograph of the bactericidal effect of CS/AgNC on the ultrastructure of *E. coli*. (A) A negative control (without CS/AgNC). (B) A treated sample (at 6 µg/ml), there are irregular-shaped rods with lysed cell walls (Ly). Also, note the separation that occurred between the bacterial cell wall membranes (arrows).

3.4. Impact of CS/AgNC on GDH and MDH enzymes and protein profiling

The effects of CS/AgNC on MDH and GDH activities of *B. cereus* and *E. coli* are shown in Figure 7 and Table 1. During the assay of MDH GDH and activities in intact and CS/AgNC-treated bacteria, it was found that the enzymatic activities and specific activities decreased after treatment. Moreover, *E. coli* was found to be more susceptible to CS/AgNC treatment than other bacterial strains. MDH activity was still present after the treatment with CS/AgNC, but it decreased from 356.9 and 566.0 to 307.1 and 36.4 µmol $NADH.min^{-1}$ for *B. cereus* and *E. coli*, respectively. Also, CS/AgNC showed vital effects on GDHs activities in the treated bacteria and decreased the specific activities of GDHs of *B. cereus* and *E. coli* from 0.274 and 0.625 to 0.250 and 0.054 µmol $NADH.min^{-1}$, respectively.

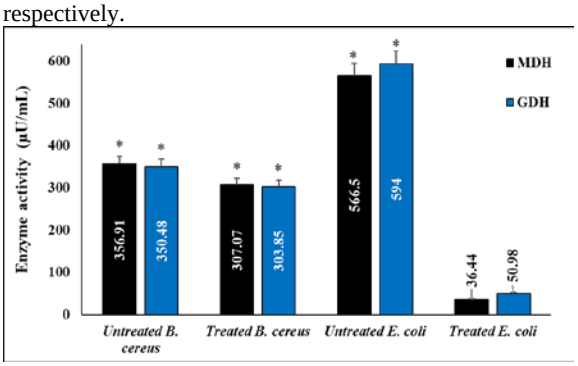

Figure 7. The enzymatic activities for MDH and GDH of the untreated and CS/AgNC-treated bacterial strains (Highly significant = * $P < 0.05$, n = 3).

Table 1. The enzymatic activities and specific activities for MDH and GDH of the untreated and CS/AgNC-treated bacterial strains (mean ± SD).

Bacterial strain	Total protein concentration (µg/ml)	GDH		MDH	
		Units of enzyme (µU/ml)	Specific activity (µU/µg)	Units of enzyme (µU/ml)	Specific activity (µU/µg)
Untreated *B. cereus*	1760 ± 0.03	350.5 ± 0.03	0.274 ± 0.03	356.9 ± 0.03	0.279 ± 0.03
Treated *B. cereus*	1900 ± 0.03	303.9 ± 0.03	0.250 ± 0.03	307.1 ± 0.03	0.253 ± 0.03
Untreated *E. coli*	1277.6 ± 0.03	549.0 ± 0.03	0.625 ± 0.03	566.0 ± 0.03	0.596 ± 0.03
Treated *E. coli*	1214.6 ± 0.03	50.9 ± 0.03	0.054 ± 0.03	36.4 ± 0.03	0.039 ± 0.03

The profile of total soluble protein revealed several changes in the protein content of treated bacteria (*B. cereus* and *E. coli*) with CS/AgNC compared with the untreated ones (Supplementary Figure 1). It was noted that some protein bands were missed at different molecular weights for the treated *B.* cereus and more bands for *E. coli*.

The MDH pattern revealed two distinct bands with approximate molecular weights of 120 and 140 kDa for both *B. cereus* and *E. coli* (Figure 8). On the other hand, the GDH isozymal pattern showed two bands with approximate molecular weights of about 130 and 170 kDa for *E. coli* and only one band (130 kDa) for *B. cereus* (Figure 9). In the case of MDH detection, the intensity of the smaller band (120 kDa) was dramatically decreased when *B. cereus* was treated with CS/AgNC, while the two bands (120 and 140 kDa) totally disappeared for the treated *E. coli*. The single band (130 kDa) of GDH did not undergo any change when *B. cereus* was treated with CS/AgNC, while the two bands (130 and 170 kDa) almost disappeared for the treated *E. coli*.

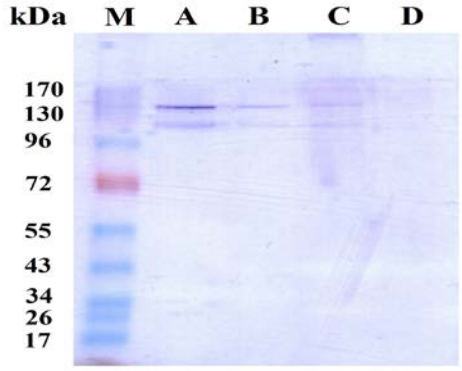

Figure 8. MDH of *B. cereus* and *E. coli* after staining at 37°C. M: marker; A: untreated *B. cereus*; B: treated *B. cereus*; C: untreated *E. coli* and D: treated *E. coli*.

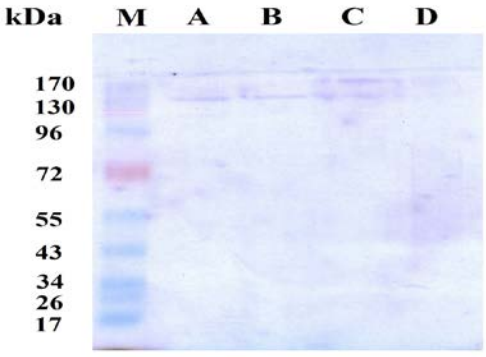

Figure 9. GDH of *B. cereus* and *E. coli* after staining at 37°C. M: marker; A: untreated *B. cereus*; B: treated *B. cereus*; C: untreated *E. coli* and D: treated *E. coli*.

4. Discussion

AgNPs have been stabilized using CS in numerous investigations (Marková *et al*., 2012; El-Sherbiny and Sedki, 2019; Bonilla *et al*., 2021). AgNPs are tightly connected to the CS OH groups, forming a network of polymeric chains that reduces NP aggregation and boosts stability (Kumar, 2000). Due to CS's antibacterial capabilities, the combination with AgNPs increased its effectiveness (An *et al*., 2018). In this study, silver nitrate was biologically reduced with *E. coli* D8 cell-free supernatant to biosynthesize AgNPs, which were then alternatively integrated into a chitosan matrix. Based on prior research demonstrating antibacterial efficacy, the bacterial supernatant was employed as reducing and stabilizing agents, respectively (Shahverdi *et al*., 2007; El-Dein *et al*., 2021). Furthermore, the presented work was also able to study the ultrastructure of CS/AgNC-treated bacteria as well as some of their enzymatic activity.

Characterization of the biosynthesized CS/AgNC, TEM, and DLS results confirmed the uniform spherical shape of AgNPs with small sizes and a high positive net surface charge that usually indicated higher antimicrobial activity, as reported previously (Ivask *et al*., 2014). AgNPs' relevance and usage are greatly influenced by their shape and size. According to reports, spherical AgNPs are the smallest in size and have the strongest antibacterial effects (Hillaireau and Couvreur, 2009; Syu *et al*., 2014). Nanomaterials' stability and propensity to aggregate are thought to be common problems that limit their potential for use in industrial and medical applications. By preventing their aggregation, the exterior capping agents are crucial in determining the shape, size, and stability of NPs (Duan *et al*., 2015). According to Siddique *et al*., (2013), the positive charge of nanometals may strengthen the attraction between particles, reducing the tendency for them to aggregate. Zeta average size and PDI values for CS/AgNC confirmed its high solubility in polar solvents, including water (Lee *et al*., 2019). The small size of metallic NPs might have a cytotoxic effect on mammalian cells (El-Zahed *et al*., 2021a). Consequently, the presented work embedded the AgNPs into the CS to decrease the silver toxicity. Also, CS participated in delaying and decreasing the silver release from its polymeric matrix.

The antibacterial activity of CS/AgNC showed a higher antibacterial action against the G-ve bacteria than the G+ve bacteria. Owaid (2018) reported that AgNPs were more effective against the G-ve than the G+ve bacteria. This difference may be due to the components and structure of the bacterial cell wall, mainly peptidoglycan thickness (Verma and Stellacci, 2010). The G-ve bacterial cell wall includes thicker and several layers of acidic compounds and lipids than the G+ve cell wall. These

acidic compounds have a strong negative charge that could bind and trap the free Ag^+ and increase its action against G-ve bacteria (Kim *et al*., 2007). The presented results agreed with previous reports confirming that the interaction of positively charged NP with cell contents has higher microbicidal action, which may be related to its easy cellular uptake and cell membrane penetration (Anas *et al*., 2013; Li *et al*., 2011). The large size of $AgNO_3$ particles might prevent its penetration throughout the bacterial cell wall, which decreased its antibacterial effects on the tested bacteria more than CS/AgNC.

CS/AgNC produced MIC values ranging from 6 µg/ml to 25 µg/ml against the tested bacterial strains in a dose-dependent manner. Nithya *et al*. (2015) reported that CS/AgNC possesses higher antibacterial activity than CS with MIC values ranging from 128 to 512 µg/ml and 16 to 128 µg/ml against *E. coli* and *S. aureus*, respectively. Arjunan *et al*., (2016) found that the CS/AgNC MIC results ranged from 8 to µg/ml against Gram-negative bacteria. MIC results of *Pongamia pinnata* seed extract-mediated green synthesized AgNPs against *S. aureus*, *E. coli*, and *B. cereus* reached to ≈250 µg/ml as documented by Paul *et al*. (2019). Also, the ultrastructure of *B. cereus* and *E. coli* after the treatment with CS/AgNC was negatively affected due to its being easily absorbed and trapped through the cell wall. The negative effects involved the inhibition of bacterial multiplication and the complete lysis of the bacterial cell or its encapsulation. Some treated cells showed a rupture between the bacterial cell membrane and its cell wall.

The negative effects of CS/AgNC on bacterial oxidative stress in its respiration were tested using two dehydrogenase enzyme behaviors; MDH and GDH (Sugimoto *et al*., 2010). An enzyme of the tricarboxylic acid cycle, MDH, occurs in most living systems. MDH catalyzes the reversible conversion of malate to oxaloacetate while reducing NAD^+ to NADH:

$$\text{L-Malate} + NAD^+ \rightleftharpoons \text{Oxaloacetate} + NADH + H^+$$

GDH catalyzes the reversible oxidation of glutamate to generate α-ketoglutarate and ammonia using NAD^+ as an electron acceptor (Plaitakis *et al*., 2017).

$$\text{Glutamate} + NAD^+ + H_2O \rightleftharpoons \text{2-Oxoglutarate} + NADH + NH_3$$

The dehydrogenase enzymes from animal cells have been extensively investigated, but information about them from bacterial sources needs more study. In *E. coli*, CS/AgNC strongly inhibited dehydrogenase activity, which was also documented by Luche *et al*. (2016). Eymard-Vernain *et al*. (2018) reported a decrease in GDH of *B. subtilis* after treatment with AgNPs and suggested that biomolecule-bearing carboxyl groups and those that are devoid of thiol groups can interact with AgNPs.

PAGE was considered one of the most sensitive methods for detecting protein and isozyme patterns. The intensity of the protein bands decreased for the treated bacteria, indicating that not only some types of protein were unexpressed, but also the level of protein expression decreased. The isozymal patterns for MDH and GDH were also performed. Selander *et al*. (1986) recorded MDH presence using electrophoresis techniques throughout different bacterial strains such as *E. coli*, *Pseudomonas aeruginosa*, *Bordetella* spp., *Hemophilus influenzae*, *Legionella pneumophila* and *Neisseria gonorrhoeae* in addition to GDH in *L. pneumophila*, *P. aeruginosa*, *N. meningitidis*, *H. influenzae*, *N. gonorrhoeae*, *Streptococcus* spp. and *Bordetella* spp. MDH and GDH patterns of CS/AgNC-treated bacteria confirmed their harmful effects on the pathogenic bacteria's dehydrogenase activity, which could reduce the pathogenicity of the bacteria or cause its death. Vineela *et al*. (2017) documented the toxic effects of AgNPs on MDH and GDH activities based on their PAGE profiles.

Overall, although both controls of the tested bacterial strains (*B. cereus*, and *E. coli*) expressed higher values of enzymatic levels, the G-ve showed more susceptibility to CS/AgNC treatment compared to the G+ve. The elimination of the bacteria may be the cause of the CS/inhibitory AgNC's effect on the respiratory enzymes MDH and GDH. Additionally, it has been proposed that Ag^+ largely influences the performance of membrane-bound enzymes that are crucial to the respiratory chain (Holt and Bard 2005). Biomolecules in the cell that include sulfur or phosphorus are more likely to react with Ag. As a result, the preferred sites for AgNPs binding are likely to be acidic compounds or sulfur-containing proteins that are found in the bacterial plasma membrane or inside the cells (Krishnaraj *et al*., 2010).

5. Conclusion

The free supernatant of *E. coli* D8 (MF062579) could act as a strong reducing agent and stabilizer in a one-step batch method to biosynthesize the CS/AgNC. This was done in the presence of sunlight. XRD, UV-visible spectrophotometry, Zeta potential, and TEM were used to confirm the synthesis of CS/AgNC. Long-term particle stability was indicated by the Zeta average size, PDI values, and AgNPs releasing properties of the CS/AgNC. With MIC values ranging from 6 to 25 g/ml, the biosynthesized nanocomposite demonstrated significant antibacterial efficacy against different G+ve and G-ve bacteria. G-ve bacteria are more sensitive to CS/AgNC than G+ve bacteria in terms of total protein content, GDH and MDH enzymes, as well as the ultrastructure of the treated bacterial cells. The presented study assumed that the biosynthesized CS/AgNC might be suitable for use it as a bacterial growth inhibitor with relatively high efficacy and stability.

References

An J, Guo G, Yin R, Luo Q, Li X, Liu F and Wang D. 2018. Facile preparation of silver/reduced graphene oxide/chitosan colloid and application of the nanocomposite in antibacterial and catalytic activity. *Polym Int*., **67**: 515-527.

Anas A, Jiya J, Rameez MJ, Anand PB, Anantharaman MR and Nair S. 2013. Sequential interactions of silver–silica nanocomposite (Ag-SiO_2NC) with cell wall, metabolism and genetic stability of *Pseudomonas aeruginosa*, a multiple antibiotic-resistant bacterium. *Lett Appl Microbiol*., **56(1)**: 57–62.

Arjunan N, Kumari HLJ, Singaravelu CM, Kandasamy R and Kandasamy J. 2016. Physicochemical investigations of biogenic chitosan-silver nanocomposite as antimicrobial and anticancer agent. *Int J Biol Macromol*., **92**: 77-87.

Badi'ah HI. 2021. Chitosan as a capping agent of silver nanoparticles. *Indones J Chem*., **9(1)**: 21-25.

Baka ZA, Abou-Dobara MI, El-Sayed AKA and El-Zahed MM. 2019. Synthesis, characterization, and antimicrobial activity of chitosan/Ag nanocomposite using *Escherichia coli* D8. *SJDFS*, **9(1)**: 1-6.

Baltazar-Encarnación E, Escárcega-González CE, Vasto-Anzaldo XG, Cantú-Cárdenas ME and Morones-Ramírez JR. 2019. Silver nanoparticles synthesized through green methods using *Escherichia coli* top 10 (Ec-Ts) growth culture medium exhibit antimicrobial properties against nongrowing bacterial strains. *J Nanomater*., **2019**: 4637325.

Bayda S, Adeel M, Tuccinardi T, Cordani M and Rizzolio F. 2020. The history of nanoscience and nanotechnology: from chemical-physical applications to nanomedicine. *Molecules*, **25(1)**: 112.

Bonilla JJA, Honorato L, Cordeiro de Oliveira DF, Araújo Gonçalves R, Guimarães A, Miranda K and Nimrichter L. 2021. Silver chitosan nanocomposites as a potential treatment for superficial candidiasis. *Med Mycol*., **59(10)**: 993-1005.

Bradford NB. 1976. A rapid and sensitive method for the quantitation microgram quantities of a protein isolated from red cell membranes. *Anal Biochem*., **72(248)**: e254.

Clinical and Laboratory Standards Institute. 2007. M100-S17. Performance standards for antimicrobial susceptibility testing; 17th informational supplement. Clinical and Laboratory Standards Institute, Wayne, PA, USA.

Clinical and Laboratory Standards Document M100-S26. 2017. Performance standards for antimicrobial susceptibility testing: Approved standard-twenty-seven Edition, Clinical and Laboratory Standards Institute, Wayne, Pennsylvania, USA.

Duan H, Wang D and Li Y. 2015. Green chemistry for nanoparticle synthesis. *Chem Soc Rev*., **44(16)**: 5778-5792.

El-Dein MMN, Baka ZA, Abou-Dobara MI, El-Sayed AK and El-Zahed MM. 2021. Extracellular biosynthesis, optimization, characterization and antimicrobial potential of *Escherichia coli* D8 silver nanoparticles. *JMBFS*, **10(4)**: 648-656.

El-Shanshoury AERR, ElSilk SE and Ebeid ME. 2011. Extracellular biosynthesis of silver nanoparticles using *Escherichia coli* ATCC 8739, *Bacillus subtilis* ATCC 6633, and *Streptococcus thermophilus* ESh1 and their antimicrobial activities. *Int Sch Res Notices*., **2011**: 385480.

El-Sherbiny IM and Sedki M. 2019. Green synthesis of chitosan-silver/gold hybrid nanoparticles for biomedical applications. In: **Pharmaceutical nanotechnology**. Humana, New York, NY, pp. 79-84.

El-Zahed MM, Baka ZA, Abou-Dobara MI, El-Sayed AK, Aboser MM and Hyder A. 2021a. *In vivo* toxicity and antitumor activity of newly green synthesized reduced graphene oxide/silver nanocomposites. *Bioresour Bioprocess*.,**8(1)**: 1–14.

El-Zahed MM, Baka Z, Abou-Dobara MI and El-Sayed A. 2021b. *In vitro* biosynthesis and antimicrobial potential of biologically reduced graphene oxide/Ag nanocomposite at room temperature. *JMBFS*, **10(6)**: e3956–e3956.

Eymard-Vernain E, Coute Y, Adrait A, Rabilloud T, Sarret G and Lelong C. 2018. The poly-gamma-glutamate of *Bacillus subtilis* interacts specifically with silver nanoparticles. *PLoS One*, **13(5)**: e0197501.

Fan X, Wang X, Cai Y, Xie H, Han S and Hao C. 2022. Functionalized cotton charcoal/chitosan biomass-based hydrogel for capturing Pb^{2+}, Cu^{2+} and MB. *J Hazard Mater*., **423**: 127191.

Genç A, Patarroyo J, Sancho-Parramon J, Bastús NG, Puntes V and Arbiol J. 2017. Hollow metal nanostructures for enhanced plasmonics: synthesis, local plasmonic properties and applications. *Nanophotonics*, **6(1)**: 193-213.

Hassanen EI and Ragab E. 2021. *In vivo* and *in vitro* assessments of the antibacterial potential of chitosan-silver nanocomposite against methicillin-resistant *Staphylococcus aureus*-induced infection in rats. *Biol Trace Elem Res*., **199(1)**: 244-257.

Hillaireau H and Couvreur P. 2009. Nanocarriers' entry into the cell: relevance to drug delivery. *Cell Mol Life Sci*., **66(17)**: 2873-2896.

Holt KB and Bard AJ. 2005. Interaction of silver (I) ions with the respiratory chain of *Escherichia coli*: an electrochemical and scanning electrochemical microscopy study of the antimicrobial mechanism of micromolar Ag^{+}. *Biochemistry*, **44(39)**: 13214-13223.

Iravani S, Korbekandi H, Mirmohammadi SV and Zolfaghari B. 2014. Synthesis of silver nanoparticles: chemical, physical and biological methods. *Res Pharm Sci*., **9(6)**: 385.

Ivask A, Kurvet I, Kasemets K, Blinova I, Aruoja V, Suppi S. and Kahru A. 2014. Size-dependent toxicity of silver nanoparticles to bacteria, yeast, algae, crustaceans and mammalian cells *in vitro*. *PloS one*, **9(7)**: e102108.

Kate S, Sahasrabudhe M and Pethe A. 2020. Biogenic silver nanoparticle synthesis, characterization and its antibacterial activity against leather deteriorates. *JJBS*., **13(4)**: 493 - 498.

Kim JS, Kuk E, Yu KN, Kim JH, Park SJ, Lee HJ and Cho MH. 2007. Antimicrobial effects of silver nanoparticles. *Nanomed: Nanotechnol Biol Med*., **3(1)**: 95-101.

Krishnaraj C, Jagan EG, Rajasekar S, Selvakumar P, Kalaichelvan PT and Mohan NJCSBB. 2010. Synthesis of silver nanoparticles using *Acalypha indica* leaf extracts and its antibacterial activity against water borne pathogens. *Colloids Surf B Biointerfaces*., **76(1)**: 50-56.

Kruger NJ. 2009. The Bradford method for protein quantitation. In: Walker JM (eds) **The Protein Protocols Handbook**. Springer protocols handbooks. Humana Press, Totowa, NJ., pp. 17-24.

Kumar MNR. 2000. A review of chitin and chitosan applications. *React Funct Polym*., **46(1)**: 1-27.

Laemmli UK. 1970. Cleavage of structural proteins during the assembly of the head of bacteriophage T4. *Nature*, **227(5259)**: 680-685.

Lee SH and Jun BH. 2019. Silver nanoparticles: synthesis and application for nanomedicine. *Int J Mol Sci*., **20(4)**: 865.

Li WR, Xie X-B, Shi Q-S, Duan S-S, Ouyang Y-S and Chen Y-B. 2011. Antibacterial effect of silver nanoparticles on *Staphylococcus aureus*. *Biometals*., **24(1)**: 135–141.

Luche S, Eymard-Vernain E, Diemer H, Van Dorsselaer A, Rabilloud T and Lelong C. 2016. Zinc oxide induces the stringent response and major reorientations in the central metabolism of *Bacillus subtilis*. *J Proteom*., **135(2016)**: 170-180.

Marková Z, Šišková K, Filip J, Šafářová K, Prucek R, Panáček A and Zbořil R. 2012. Chitosan-based synthesis of magnetically-driven nanocomposites with biogenic magnetite core, controlled silver size, and high antimicrobial activity. *Green Chem*., **14(9)**: 2550-2558.

Menazea AA, Eid MM and Ahmed MK. 2020. Synthesis, characterization, and evaluation of antimicrobial activity of novel chitosan/tigecycline composite. *Int J Biol Macromol*., **147**: 194-199.

Namasivayam SKR, Pattukumar V, Samrat K, Kumar JA, Bharani RA, Alothman AA, Osman SM, Tran VA and Rajasimman M. 2022. Evaluation of methyl orange adsorption potential of green synthesized chitosan-silver nanocomposite (CS–AgNC) and its notable biocompatibility on freshwater Tilapia (*Oreochromis nitoticus*). *Chemosphere*, **308(2)**: 135950.

Natsuki J, Natsuki T and Hashimoto Y. 2015. A review of silver nanoparticles: synthesis methods, properties and applications. *Int j mater sci*., **4(5)**: 325-332.

Nguyen NTT, Nguyen LM, Nguyen TTT, Tran UP, Nguyen DTC and Van Tran T. 2022. A critical review on the bio-mediated green synthesis and multiple applications of magnesium oxide nanoparticles. *Chemosphere*, **312(1)**: 137301.

Nithya A, JeevaKumari HL, Rokesh K, Ruckmani K, Jeganathan K and Jothivenkatachalam K. 2015. A versatile effect of chitosan-silver nanocomposite for surface plasmonic photocatalytic and antibacterial activity. *J Photochem Photobiol B: Biol*., **153**: 412-422.

O'connor BP. 2000. SPSS and SAS programs for determining the number of components using parallel analysis and Velicer's MAP test. *Behav Res Methods Instrum Comput*., **32(3)**: 396-402.

Owaid MN, Muslim RF and Hamad HA. 2018. Mycosynthesis of silver nanoparticles using *Terminia* sp. desert truffle, pezizaceae, and their antibacterial activity. *JJBS*., **11(4)**: 401-405.

Paul M and Londhe VY. 2019. *Pongamia pinnata* seed extract-mediated green synthesis of silver nanoparticles: Preparation, formulation and evaluation of bactericidal and wound healing potential. *Appl Organomet Chem*., **33(3)**: e4624.

Plaitakis A, Kalef-Ezra E, Kotzamani D, Zaganas I and Spanaki C. 2017. The glutamate dehydrogenase pathway and its roles in cell and tissue biology in health and disease. *Biology*, **6(1)**: 11.

Price GJ, White AJ and Clifton AA. 1995. The effect of high-intensity ultrasound on solid polymers. *Polymer*., **36(26)**: 4919-4925.

Restrepo CV and Villa CC. 2021. Synthesis of silver nanoparticles, influence of capping agents, and dependence on size and shape: A review. *Environ Nanotechnol Monit Manag*., 100428.

Robb FT, Maeder DL, Diruggiero J, Borges KM and Tolliday N. 2001. Glutamate dehydrogenases from hyperthermophiles. In: **Methods in enzymology** (Vol. 331). Academic Press, pp. 26-41.

Saravanan A, Kumar PS, Karishma S, Vo DVN, Jeevanantham S, Yaashikaa PR and George CS. 2021. A review on biosynthesis of metal nanoparticles and its environmental applications. *Chemosphere*, **264**: 128580.

Selander RK, Caugant DA, Ochman H, Musser JM, Gilmour MN and Whittam TS. 1986. Methods of multilocus enzyme electrophoresis for bacterial population genetics and systematics. *Appl Environ Microbiol*., **51(5)**: 873-884.

Shahverdi AR, Minaeian S, Shahverdi HR, Jamalifar H and Nohi AA. 2007. Rapid synthesis of silver nanoparticles using culture supernatants of *Enterobacteria*: a novel biological approach. *Process Biochem*., **42(5)**: 919-923.

Siddique YH, Fatima A, Jyoti S, Naz F, Khan W, Singh BR and Naqvi AH. 2013. Evaluation of the toxic potential of graphene copper nanocomposite (GCNC) in the third instar larvae of transgenic *Drosophila melanogaster* (hsp70-lacZ) Bg9. *PloS One*, **8(12)**: e80944.

Singh A, Gautam PK, Verma A, Singh V, Shivapriya PM, Shivalkar S, Sahoo AK and Samanta SK. 2020. Green synthesis of metallic nanoparticles as effective alternatives to treat antibiotics resistant bacterial infections: A review. *Biotechnol Rep*., **25**: e00427.

Sotiriou GA, Meyer A, Knijnenburg JT, Panke S and Pratsinis SE. 2012. Quantifying the origin of released Ag^+ ions from nanosilver. *Langmuir*, **28(45)**: 15929-15936.

Sugimoto S, Higashi C, Matsumoto S and Sonomoto K. 2010. Improvement of multiple-stress tolerance and lactic acid production in *Lactococcus lactis* NZ9000 under conditions of thermal stress by heterologous expression of *Escherichia coli* dnaK. *Appl Environ Microbiol*., **76(13)**: 4277-4285.

Syu YY, Hung JH, Chen JC and Chuang HW. 2014. Impacts of size and shape of silver nanoparticles on *Arabidopsis* plant growth and gene expression. *Plant Physiol Biochem*., **83**: 57-64.

Tripathi S, Mehrotra GK and Dutta PK. 2011. Chitosan-silver oxide nanocomposite film: Preparation and antimicrobial activity. *Bull Mater Sci*., **34(1)**: 29-35.

Tsekhmistrenko SI, Bityutskyy VS, Tsekhmistrenko OS, Horalskyi LP, Tymoshok NO and Spivak MY. 2020. Bacterial synthesis of nanoparticles: A green approach. *Biosyst Divers*., **28(1)**: 9-17.

Verma A and Stellacci F. 2010. Effect of surface properties on nanoparticle-cell interactions. *Small*, **6(1)**: 12–21.

Vineela D, Reddy SJ and Kumar BK. 2017. Impact of *Lihocin* and *Aeromonas veronii* on metabolic biomarkers of fish *Catla catla* against to immunostimulant silver nanoparticles. *Int J Pharma Bio Sci*., **4(1)**: 38-46.

Yoshida A. 1965. Enzymic properties of malate dehydrogenase of *Bacillus subtilis*. *JBC*, **240(3)**: 1118-1124.

Youssef K and Hashim AF. 2020. Inhibitory effect of clay/chitosan nanocomposite against *Penicillium digitatum* on citrus and its possible mode of action. *JJBS*, **13(3)**: 349 - 355.

Yuan Q, Hein S and Misra RDK. 2010. New generation of chitosan-encapsulated ZnO quantum dots loaded with drug: synthesis, characterization and *in vitro* drug delivery response. *Acta Biomater*., **6(7)**: 2732-2739.

Zhang XF, Liu ZG, Shen W and Gurunathan S. 2016. Silver nanoparticles: synthesis, characterization, properties, applications, and therapeutic approaches. *Int J Mol Sci*., **17(9)**: 1534.

Supplementary

Table 1. The Zeta average size and poly dispersity index for CS/AgNC.

Solvent	Zavg (nm)	PDI (d.nm)
Water	313	0.394
Methanol	841	0.745
Ethanol	444	0.632
DMF	370	0.420
n-butyl alcohol	312	0.400
Acetone	1711	0.801
Toluene	1145	0.896
Hexane	647	0.688

Table 2. The Zeta average size and poly dispersity index for CS/AgNC.

Antibacterial agent	Zone of inhibition (n=3, mm, mean ± SE)	
	B. cereus ATCC 6633	*E. coli* ATCC 25922
$AgNO_3$	15 ± 0.06	21 ± 0.03
CS	13 ± 0.14	25 ± 0.06
AgNPs	19 ± 0.06	26 ± 0.03
CS/AgNC	25 ± 0.06	35 ± 0.03
Penicillin	20 ± 0.14	39 ± 0.03

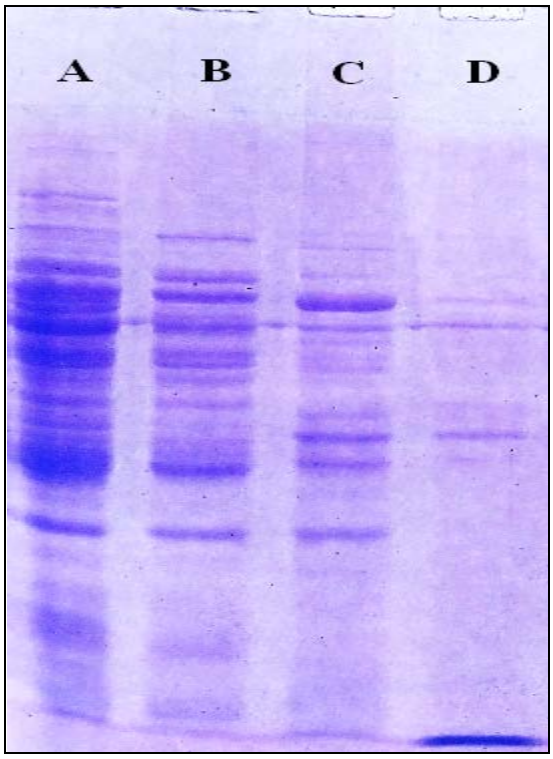

Figure 1. Protein expression profile on SDS-PAGE of *B. cereus* and *E. coli*. A: untreated *B. cereus*; B: treated *B. cereus*; C: untreated *E. coli* and D: treated *E. coli*. The gel was stained with Coomassie blue.